Journal of Energy Chemistry 41 (2020) 135–141

Contents lists available at ScienceDirect

Journal of Energy Chemistry

journal homepage: www.elsevier.com/locate/jechem

http://www.journals.elsevier.com/journal-of-energy-chemistry/

Understanding of performance degradation of $LiNi_{0.80}Co_{0.10}Mn_{0.10}O_2$ cathode material operating at high potentials

Sheng S. Zhang*

Electrochemistry Branch, FCDD-RLS-DC, Sensors and Electron Devices Directorate, U.S. Army Research Laboratory, Adelphi, MD 20783-1138, USA

ARTICLE INFO

Article history:
Received 1 April 2019
Revised 23 April 2019
Accepted 20 May 2019
Available online 25 May 2019

Keywords:
Ni-rich cathode
Lattice oxygen
Phase transition
Oxygen evolution
Performance degradation

ABSTRACT

Inferior cycling stability, poor safety, and gas generation are long lasting problems of Ni-rich $LiNi_{0.80}Co_{0.10}Mn_{0.10}O_2$ (NCM811) cathode material. Although much effort has been made, mechanisms for the above problems are poorly understood. Studying the cycling and float-charging characteristics of Li/NCM811 cells in high voltage conditions (4.5 V and 4.7 V, respectively), in this work we find that nearly all known problems with NCM811 material can be attributed to the oxidation of lattice oxygen occurring in the capacity region corresponding to H2 → H3 phase transition. While contributing to overall capacity, the oxidation of lattice oxygen results in a loss of oxygen through oxygen evolution and relative reactions between active oxygen evolution intermediates and electrolyte solvents. It is the loss of oxygen that results in irreversible layered-spinel-rocksalt phase transition, secondary particle cracking, and performance degradation. The conclusions of this work suggest that the priority for further research on NCM811 material should give to the suppression of oxygen evolution, followed by the use of the anti-oxygen electrolyte being chemically stable against the active oxygen evolution intermediates.

Published by Elsevier B.V. and Science Press on behalf of Science Press and Dalian Institute of Chemical Physics, Chinese Academy of Sciences.

1. Introduction

Ni-rich $LiNi_{0.80}Co_{0.10}Mn_{0.10}O_2$ (NCM811) has recently attracted much attention for developing high energy density Li-ion batteries because of its high specific capacity and high operating potential [1–4]. In this material, each type of transition metal ions plays its particular roles, that is, Ni ions contribute to the majority of capacity through the Ni^{2+}/Ni^{3+} and Ni^{3+}/Ni^{4+} redox couples, Co ions suppress Ni/Li cationic mixing in the synthesis and cycling while increasing rate capability, and Mn ions stabilize the structure and enhance thermal stability by remaining at +4 valence to act as a structural stabilizer [5,6]. Unfortunately, the implementation of NCM811 in commercial Li-ion batteries is still hindered by its inferior cycling stability, poor thermal stability (safety issue), and gas generation. Although poorly understood, several mechanisms have been proposed to explain the performance degradation of NCM materials, including irreversible phase transition [6–11], oxygen evolution [12,13], secondary particle cracking [14–17], as well as residual Li compounds [5,18–20]. Without exception, all the above mechanisms are linked to the operation and/or storage of batteries in high voltage conditions (i.e., >4.3 V vs. Li/Li^+ in the potential of the cathode). Since tetravalent nickel and cobalt oxides (MO_2, M = Ni and Co) are thermodynamically instable, the delithiated (charged) NCM811 is subject to spontaneous transformation from the layered phase ($R\bar{3}m$) over disordered spinel phase ($Fd\bar{3}m$) to the NiO-like rocksalt phase (Fm3m) [6–8], and becomes very unstable at high temperature [21,22]. The layered-spinel-rocksalt phase transition on one hand reduces M^{4+} ions to much stable M^{2+} ions, resulting in a loss in the capacity, and on the other hand produces active oxygen [23,24]. Both the delithiated MO_2 [15,25] and active oxygen [12,13] can chemically oxidize electrolyte solvents, resulting in electrolyte depletion, gas generation, and a rise in the cell's impedance. In addition, oxygen evolution [26] and anisotropic unit-cell volume change [14,17,27] in cycling were reported to be responsible for the formation of microcracks in NCM secondary particles. Electrolyte penetration into microcracks and resultant reaction with the delithiated cathode produces resistive surface layer on the crack surface, which adds extra barrier for the diffusion of Li^+ ions. Residual lithium compounds (Li_2CO_3, LiOH, and Li_2O) introduced in the synthesis for suppressing Li/Ni cationic mixing and also formed during storage in ambient atmosphere were identified to be another source for the gas generation. It was reported that the residual lithium compounds can be electrochemically oxidized at potentials higher than 4.3 V vs. Li/Li^+, generating CO_2 and superoxide anodic radicals [28–30], of which the latter

* Corresponding author.
E-mail addresses: shengshui.zhang.civ@mail.mil, shengshui@gmail.com

https://doi.org/10.1016/j.jechem.2019.05.013
2095-4956/Published by Elsevier B.V. and Science Press on behalf of Science Press and Dalian Institute of Chemical Physics, Chinese Academy of Sciences.

further react with electrolyte solvents to produce more gaseous products.

Early studies by various types of transmission electron microscopies revealed that the layered-spinel-rocksalt phase transition is limited to near surface of the cathode particles, typically 10–25 nanometers in depth [12,29,31–33]. However, recent studies showed that such phase transitions can overspread towards the bulk of the cathode particles in operation and/or storage [10,29,34,35]. This finding suggests that further works are needed to understand the mechanism for the performance degradation of NCM materials. For this reason, in this work we studied changes in the profile of differential capacity vs. cell's voltage under different cycling conditions. With the aid of X-ray diffraction characterization on the cycled cathode and combining the observations of previous publications, we concluded that oxygen loss is the key origin for irreversible layered-spinel-rocksalt phase transition and NCM811 secondary particle cracking, and that the oxidation of lattice oxygen is an intrinsic nature of NCM811 material at high potentials or high temperatures. Our conclusion suggests that future research on the NCM811 cathode material should give priority to suppression of the oxygen evolution, and development of the anti-oxygen electrolytes that are chemically stable against the active oxygen evolution intermediates.

2. Experimental

NCM811 powder, provided by Targray, Canada, was coated onto an aluminum foil in composition of 80% NCM811, 10% Super-P carbon black, and 10%, polyvinylidene fluoride by using N-methyl-2-pyrrolidone as the solvent. Resulting cathode was punched into circular disks with a 1.27 cm^2 area, and dried at 110 °C under vacuum for 16 h. On average, the loading of NCM811 on the cathode was 8.0–8.2 mg cm^{-2}. A solution of 1.0 mol kg^{-1} $LiPF_6$ dissolved in a 3:7 (w:w) mixture of ethylene carbonate and ethyl methyl carbonate was used as the electrolyte, and constant amount of 40 μL electrolyte was added in all cells. Using two pieces of Celgard 2400 membranes as the separator, Li/NCM811coin cells were assembled and activated by charging and discharging at 0.1 C between 3.0 V and 4.7 V for one cycle unless noted otherwise. The cells were cycled on a Maccor Series 4000 tester at 0.5 C by charging the cell to cutoff voltage and then holding at the cutoff voltage until the current declined to 0.1 C. The C rate was referenced to a specific capacity of 200 mAh g^{-1} NCM811.

AC impedance of the cells was measured at 20 °C by a Solartron SI 1287 Electrochemical Interface in combination with a Solartron SI 1260 Impedance/Gain-Phase Analyzer. In measurement, the newly-assembled cell was charged at 0.1 C to testing voltage (4.5 V and 4.7 V, respectively), followed by holding the cell at the testing voltage and measuring the cell's impedance in different float-charging time intervals. AC-impedance was measured with a DC polarization (4.5 V or 4.7 V, respectively) and a 10 mV AC-perturbation in frequency range from 100,000 Hz to 0.01 Hz. To prepare the sample for X-ray diffraction (XRD) characterization, the cycled/tested cathode was harvested and rinsed using ethyl methyl carbonate in a glove-box, followed by drying at 100 °C under vacuum overnight. The XRD pattern of the samples was acquired by a Rigaku MiniFlex600 X-ray diffractometer.

3. Results and discussion

Fig. 1(a) shows voltage profile of the initial three cycles for a Li/NCM811 cell. It is observed that voltage profile of the 1st cycle largely differs from other two by its higher polarization in the initial charging period and lower coulombic efficiency in the cycling. This is a common phenomenon for all types of NCM cathode materials, and it can be attributed to the inhomogeneous grain boundary contact in the original state of NCM material for the higher polarization and the Li/Ni cationic mixing occurring in the initial charging process for the lower coulombic efficiency. In particular, the Li/NCM811 cell shows a broad differential charging capacity peak stating at 4.33 V in the first charging, and accordingly a sharp differential discharging capacity peak at 4.53 V in the subsequent discharging, as indicated in the inset of Fig. 1(b). Since the electrolyte used in this work can be electrochemically stable up to 5.0 V vs. Li/Li^+ on the Super-P carbon [24,36], the above two differential capacity peaks are more reasonably assigned to the residual Li compounds (Li_2CO_3, LiOH, and Li_2O) for charging and the chemisorbed active oxygen for discharging on the NCM811 surface [5,18–20]. It was reported that the residual Li compounds can be electrochemically oxidized above 4.3 V vs. Li/Li^+ through Eqs. (1)–(3) [28–30,37], and that these reactions are poorly reversible because of the parasitic reactions between the oxygen redox intermediates and electrolyte solvents [38,39].

$$Li_2O - 2e^- \rightarrow \tfrac{1}{2}O_2 + 2Li^+ \quad (1)$$

$$LiOH - 2e^- \rightarrow \tfrac{1}{2}O_2 + Li^+ + H^+ \quad (2)$$

$$Li_2CO_3 - 2e^- \rightarrow \tfrac{1}{2}O_2 + CO_2 + 2Li^+ \quad (3)$$

The above assignment is well evidenced by the vanishing of these two differential capacity peaks in the 2nd cycle, and therefore it can be concluded that the residual Li compounds affect gas generation mainly in the initial formation cycle.

Fig. 2 exhibits a typical profile of the plots of differential capacity vs. cell's voltage for Li/NCM811 cells. It is clearly observed that the capacity of NCM811 material is contributed by four-step phase transition in the order of voltage increasing from hexagonal (H1) through monoclinic (M) to hexagonal (H2 and H3) [5,12,40]. Since the $Co^{4+/3+}$ redox couple contributes to small part of capacities, differential capacity peak of the H1→M transition is often split into two overlapped peaks. Of particular importance for the capacity retention and thermal stability of NCM811 material, the H2→H3 phase transition above 4.11 V is inevitably accompanied by the oxidation of lattice oxygen, and it experiences much large change in the unit-cell volume [5,27], resulting in NCM811 secondary particle cracking. Therefore, the capacity region corresponding to the H2→H3 transition is considered to be instable as distinguished by the color in Fig. 2. In this region, the capacity and reversibility of NCM811 are affected by both of the H2→H3 phase transition and the lattice oxygen redox [35,41–44], and the similar conclusions have been well documented on the Li-rich layered cathode materials [22,45,46]. The above partition on the capacity region can be supported by the following facts: (1) oxygen evolution initiates at 4.3 V vs. Li/Li^+ and becomes significant above 4.55 V [12,24], (2) oxygen evolution is simultaneously accompanied by the generation of CO_2 and CO as a result of the chemical reactions between the active oxygen evolution intermediates and electrolyte solvents [12,13,47], (3) the ultimate delithiation products are thermodynamically instable so that up to date neither pure NiO_2 nor pure CoO_2 has been prepared/reported, and (4) there is a delay, even by an *operando* technique, in the time (and further the potential) between oxygen evolution and detection by the instrument due to the need for the diffusion of oxygen molecules from the lattice to the surface of NCM811 particles. In the thermodynamic view, the oxidation of lattice oxygen can be understood by the following two chemical equilibriums [6,12,43].

$$MO_2(\text{layered}) \rightleftharpoons M_3O_4(\text{spinel}) + [O] \quad (4)$$

$$M_3O_4(\text{spinel}) \rightleftharpoons MO(\text{rocksalt}) + [O] \quad (5)$$

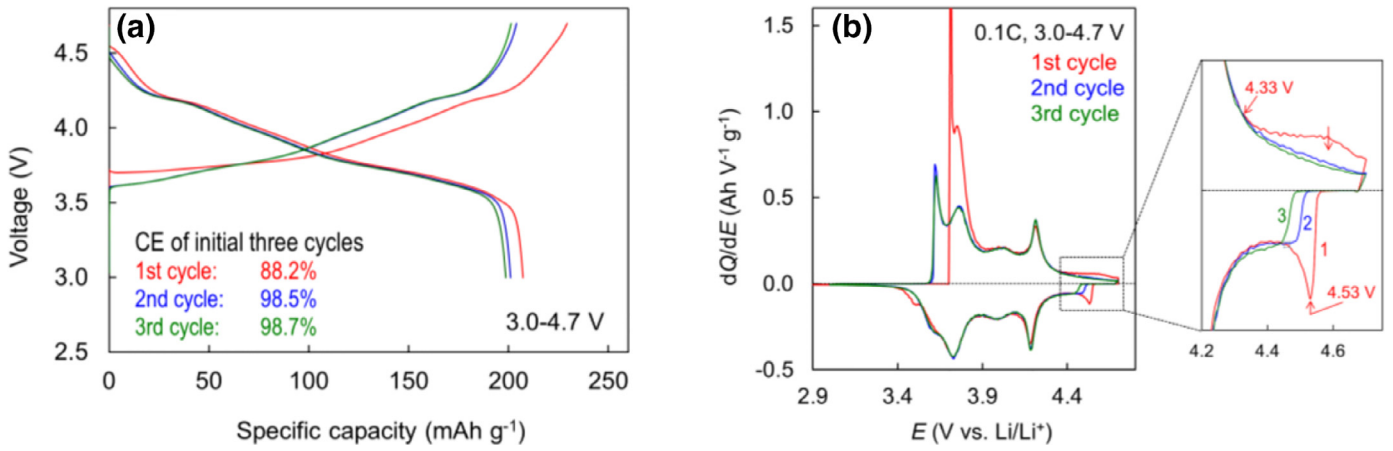

Fig. 1. Electrochemical characteristic of the initial three cycles of Li/NCM811 cells, recorded at 0.1 C in 3.0–4.7 V. (a) Voltage profile, and (b) plot of differential capacity vs. cell voltage.

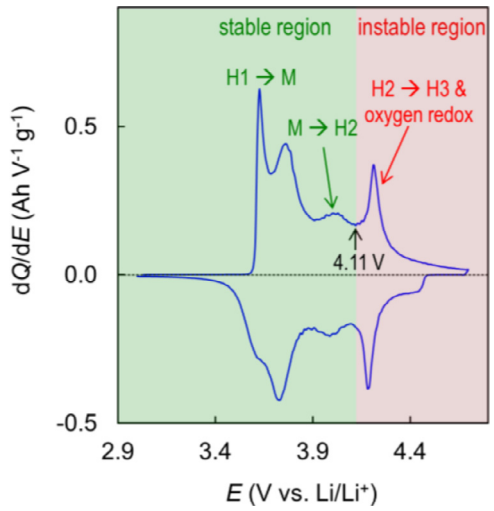

Fig. 2. Typical pattern of the differential capacity vs. cell's voltage for Li/NCM811 cells.

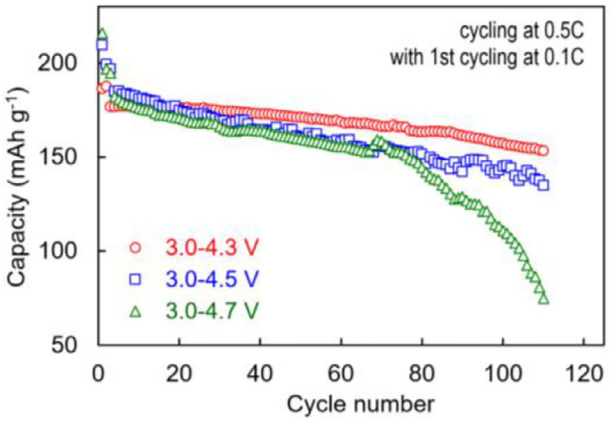

Fig. 3. Cycling performance of Li/NCM811 cells in different voltage ranges.

Where [O] represents active oxygen intermediates, which may be any forms of the excited state singlet oxygen ($^1O_2$), peroxide anodic radicals ($O–O^{\bullet-}$), and peroxide bonds (O–O) between the transition metal ions [12,24,28–30]. While contributing to overll capacity, the active oxygen can be either self-quenched by combining into the ground state oxygen molecules (i.e., so-called oxygen evolution) or reacted with the electrolyte solvents, resulting in gas generation and a rise in the cell's impedance. In our view, nearly all known problems with NCM811 material can be attributed to the oxygen evolution and its relative reactions between the active oxygen evolution intermediates and electrolyte solvents, both of which result in a net loss of oxygen. It is the loss of oxygen that results in irreversible layered-spinel-rocksalt phase transition and secondary particle cracking of NCM811 material. According to the above conclusions, research priority for solving the problems of NCM811 material should give to suppression of the oxygen evolution, followed by development of the anti-oxygen electrolytes that are chemically stable against the active oxygen evolution intermediates. In this regard, cationic doping has been proven to be particularly effective in stabilizing the lattice structure of layered transition metal oxides [48–52], and nonflammable electrolytes would be a good option because of their ability in retarding the propagation of oxygen radicals [53,54].

Cycling performances of three Li/NCM811 cells in different voltage ranges are compared in Fig. 3. It can be seen that raising the charging cutoff voltage does not significantly increase specific capacity, instead that the capacity retention deteriorates with an increase in the charging cutoff voltage. As such, the cell cycled in the 3.0–4.3 V range retained the highest capacity in the end of testing (110 cycles). Since the cell's energy density (mWh g^{-1}) equals to the product of specific capacity (mAh g^{-1}) and average operating voltage (V), the voltage profile and differential capacity plot of these three cells are representatively compared in Fig. 4. Without exception, the cells' capacity and discharging voltage are declined with the cycle number, and the fading rate accelerates with an increase in the charging cutoff voltage (Figs. 4a, c, and e). Comparing the profile of differential capacity sheds deep insight into the performance degradation (Figs. 4b, d and f). It is distinctly observed that decline in the discharging voltage with the cycle number is attributed to not only an increase in the ohmic polarization, but also a change in the phase structure of NCM811 material as evidenced by decreases in the number and voltage of the differential capacity peaks. Particularly for the discharging process (Fig. 4f), the cell had three differential discharging capacity peaks in the 5th and 20th cycles, however, decreased to two peaks in the 50th and 100th cycles with vanishing of the peak corresponding to the H3→H2 phase transition. More importantly, the peak voltage of differential discharging capacity declined with an increase in the cycle number. Similar results are also observed from the 3.0–4.3 V range (Fig. 4b) and 3.0–4.5 V range (Fig. 4d) except for a relatively slow fading rate. Vanishing of the differential capacity peak corresponding to the H3→H2 phase transition is excellent evidence for the irreversible layered-spinel-rocksalt phase transition of NCM811 material [6–8]. Due to the loss of oxygen, the average

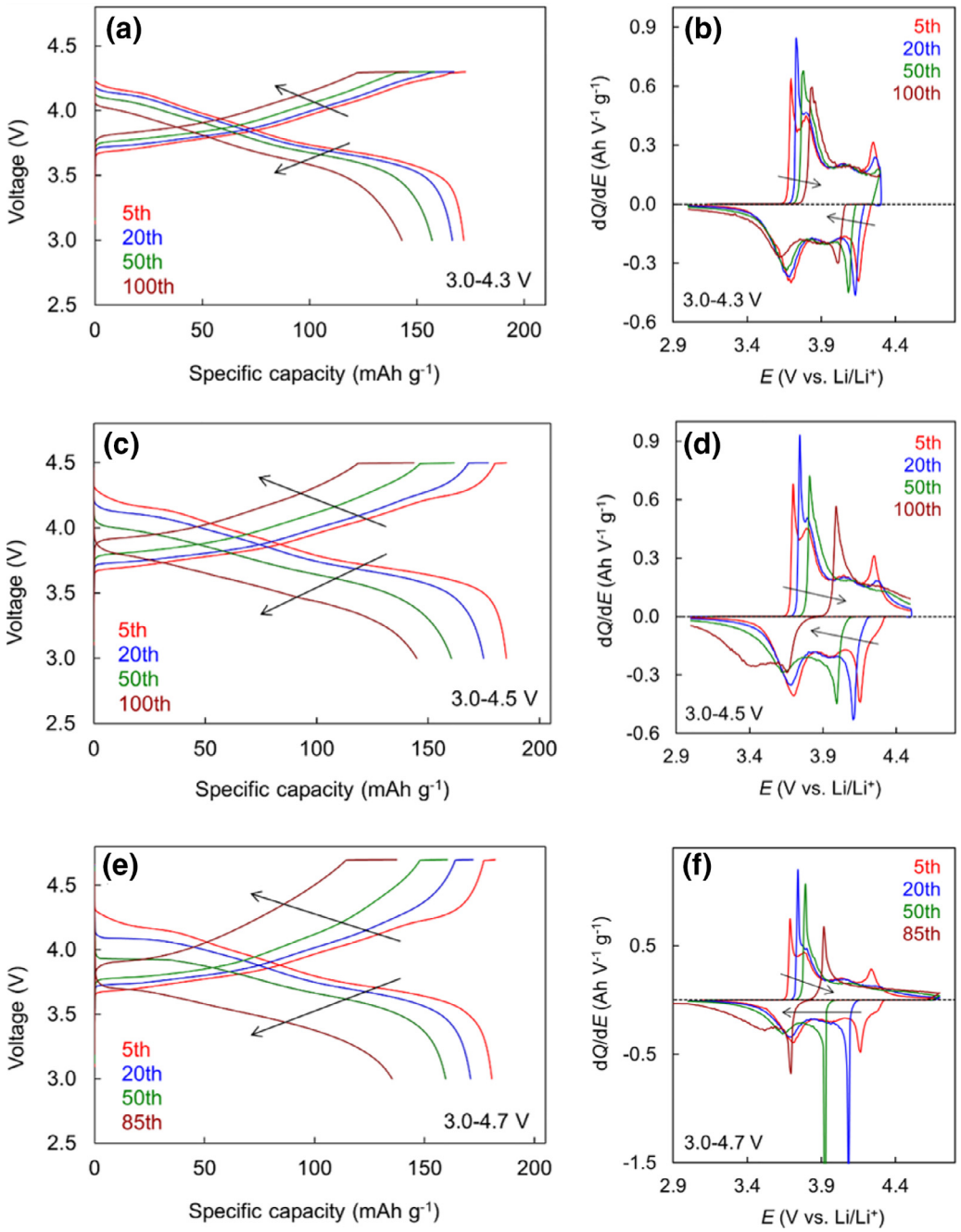

Fig. 4. Selective profiles for the cell's voltage and differential capacity of Li/NCM811 cells cycled in different voltage ranges. (a & b) 3.0–4.3 V, (c & d) 3.0–4.5 V, and (e & f) 3.0–4.7 V.

valence of transition metals in the spinel and rocksalt phases is accordingly lowered, resulting in decreases in the operating voltage and specific capacity of NCM811 material [46].

Fig. 5 compares voltage profile and differential capacity plot of two Li/NCM811 cells subject to different float-charging conditions, in which two newly assembled cells were charged at 0.1 C to 4.7 V, followed by holding the cell at 4.7 V for 1 h and 200 h, respectively. After float-charging, the cells were discharged at 0.1C to 3.0 V, leading to almost same capacity, i.e., 203 mAh g^{-1} for the 1 h float-charging and 205 mAh g^{-1} for the 200 h float-charging. However, the 200 h float-charging had much lower coulombic efficiency (72.0% vs. 87.3% of the 1 h float-charging, as noted in Fig. 5a), but had a little higher discharging voltage in the 3.8–4.2 V region as marked by the shadow area. The former suggests that extended float-charging time at 4.7 V leads to redox shuttle of the soluble active oxygen intermediates because electrochemical oxidation of the electrolyte solvents at 4.7 V vs. Li/Li^+ occurs mainly in the initial several hours (to be discussed later). The soluble active oxygen intermediates with paramagnetism have been experimentally detected from a Co_3O_4-catalyzed Li/Li_2O cell by the electron spin resonance spectroscopy [55], and supported by the fact that the thermal runway of NCM-based Li ion batteries can be triggered without need of internal electric shorting (i.e., separator melting), instead by the reaction of the lithiated graphite and the active oxygen that is released from the delithiated NCM cathode, dissolved into the liquid electrolyte, and diffused into the anode [56]. The latter suggests that degradation of the delithiated cathode is a self-decomposition process as proposed by Eqs. (4) and 5, other

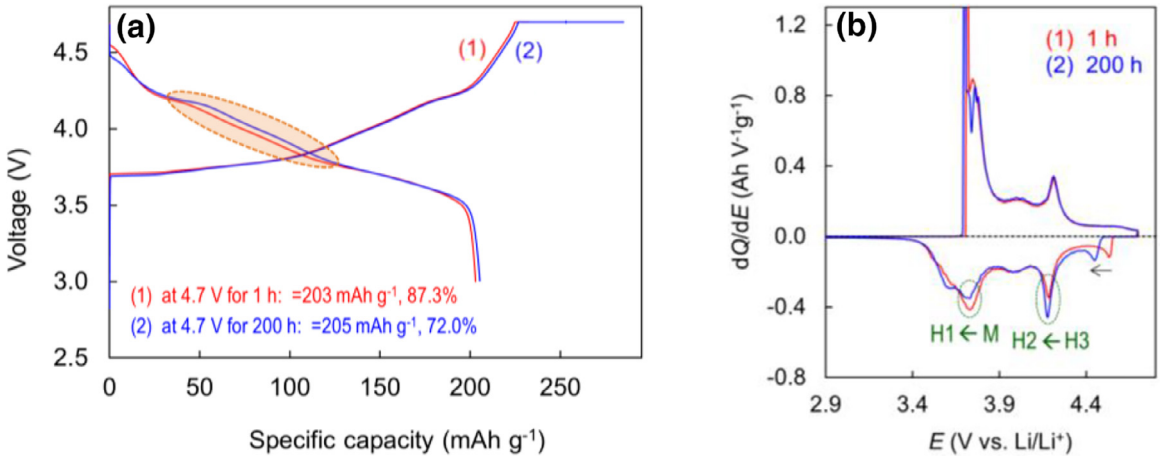

Fig. 5. Effect of float-charging time at 4.7 V on electrochemical characteristic of the initial cycle. (a) Voltage profile, and (b) differential capacity.

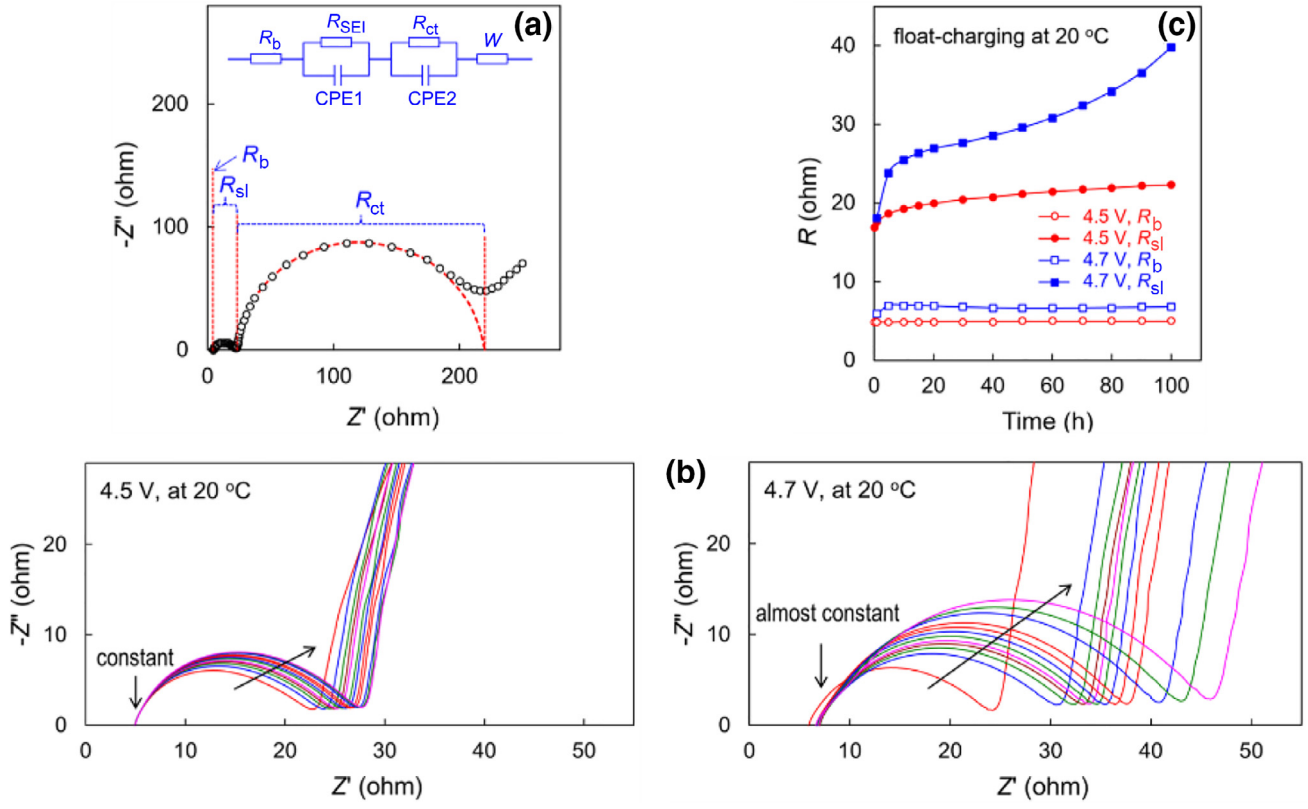

Fig. 6. (a) Typical impedance spectrum of Li cells and equivalent circuit used for fitting of electric elements, (b) change of impedance spectrum with float-charging time at 4.5 V and 4.7 V, respectively, in the initial charging, and (c) comparison of the growth of R_b and R_{sl} during float-charging at 4.5 V and 4.7 V, respectively, where the slope arrow shows an increase in the float-charging time.

than a process of the reaction between the delithiated cathode and electrolyte solvents. Of interest, the values of the discharging differential capacity peaks for the H3→H2 and M→H1 transitions are in reversal order for the 1 h and 200 h float-charging (see two circles in Fig. 5b). This provides excellent evidence for the contribution of lattice oxygen redox to overall capacity, and it is affected by the float-charging time. In addition, it is shown by the horizontal arrow in Fig. 5(b) that after float-charging at 4.7 V for 200 h, the differentical discharging capacity peak of the active oxygen generated by the residual Li compounds was shifted to a little lower. This is probably because the activity of active oxygen species gradually decays with the time as the common radicals do.

The effect of float-charging time was further studied by AC-impedance analysis, and the results are summarized in Fig. 6, in which (a) shows a typical impedance spectrum of the Li metal cells and an equivalent circuit suitable for fitting of electric elements. Briefly, the impedance of a Li metal cell is composed mainly of bulk resistance (R_b), surface layer resistance (R_{sl}), and charge-transfer resistance (R_{ct}), in which the R_{sl} and R_{ct} are usually reflected by two overlapped semicircles [57,58]. The R_{ct}, a measure of the cell's electrode reaction kinetics, is a function of the cell's state-of-charge, and it theoretically approaches indefinite large without forming a semicircle near the charging and discharging ends. Therefore, the part of the impedance spectra corresponding

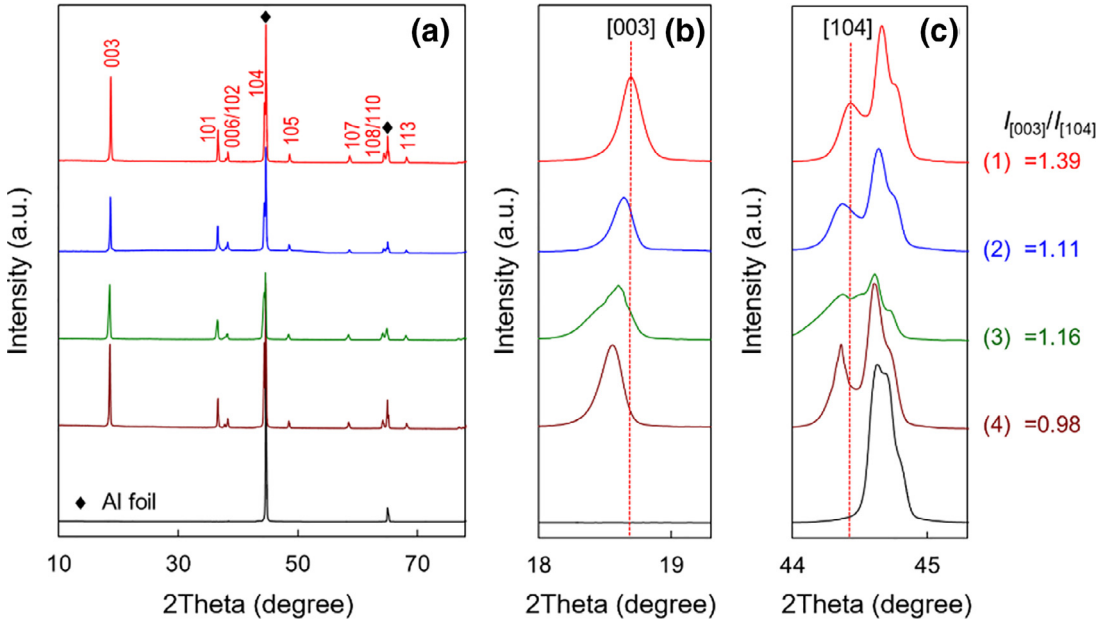

Fig. 7. XRD pattern of NCM811 cathodes. (1) Pristine cathode, (2) after 200 cycles at 0.5 C in 3.0–4.5 V, (3) after float-charging at 4.5 V for 200 h, and (4) after float-charging at 4.7 V for 200 h. Note that Samples (2), (3) and (4) were obtained by discharging the cell at 0.1 C to 3.0 V, and that the bottom pattern is Al current collector for reference and the right two panels are enlargement of the [003] peak and [104] peak, respectively.

to the R_b and R_{sl} was analyzed in the present work. The spectra of two Li/NCM811 cells for various float-charging times at 4.5 V and 4.7 V, respectively, are plotted together in Fig. 6(b), showing such a general trend that the semicircle's diameter progressively grows with the float-charging time. Using the equivalent circuit shown in the inset of Fig. 6(a), the R_b and R_{sl} are fitted and plotted as a function of the float-charging time in Fig. 6(c). It is interesting to observe that in both cases, the R_b remains constant except for the first 5 h in the 4.7 V float-charging whereas the R_{sl} progressively increases with the float-charging time. The above observation indicates that at 4.7 V vs. Li/Li$^+$ electrochemical oxidation of the electrolyte solvents and its resulting increase in the R_{sl} occur mostly in the initial 5 h period or the initial charging, and that further increase in the R_{sl} is mainly attributed to the irreversible layered-spinel-rocksalt phase transition of NCM811 material, resulting in the formation of a low conductive surface reconstruction layer on the NCM811 particles.

The layered-spinel-rocksalt phase transition was further verified by the change in crystalline structure of NCM811 material. Fig. 7 compares the XRD patterns of the pristine NCM811 cathode and three tested NCM811 cathodes under different testing conditions. Overall, the layered structure of NCM811 material was fairly retained in Samples (2), (3), and (4), which were subjected to cycling at 0.5 C in 3.0–4.3 V for 200 cycles, float-charging at 4.5 V for 200 h, and float-charging at 4.7 V for 200 h, respectively. Paying attention to the [003] and [104] peaks (the right two panels in Fig. 7) finds that after galvanostatic cycling and float-charging tests, these two peaks slightly shifted towards low 2θ values, suggesting a small change in the lattice parameters of NCM811 material. As a measure of the Ni/Li disorder in the layered NCM cathode materials [59–61], the $I_{[003]}/I_{[104]}$ intensity ratio was calculated to be 1.39, 1.11, 1.16, and 0.98 for the pristine cathode, Samples (2), (3), and (4), respectively. Compared with the pristine cathode ($I_{[003]}/I_{[104]} = 1.39$), a decrease in the $I_{[003]}/I_{[104]}$ ratio for Samples (2), (3), and (4) indicates that all these three cathodes suffered in different degrees layered-spinel-rocksalt phase transition as a result of the loss of oxygen, as suggested by Eqs. (4) and 5.

4. Conclusions

In summary, performance degradation of the Li/NCM811 cells in high voltage (>4.3 V) operation was studied by galvanostatic cycling and float-charging tests in combination with the post-mortem analysis on the tested cathode using the XRD technique. It is shown that the H2→H3 phase transition in the voltage above 4.1 V is inevitably accompanied by the oxidation of lattice oxygen. While contributing to overall capacity, the oxidation of lattice oxygen triggers oxygen evolution during which the active oxygen evolution intermediates, such as excited state singlet oxygen ($^1O_2$), peroxide anodic radicals ($O-O^{\bullet-}$) and peroxide bonds (O–O), chemically oxidize the electrolyte solvents, resulting in gas generation and a rise in the cell's impedance. The loss of oxygen results in irreversible layered-spinel-rocksalt phase transition and a decrease in the average valence of transition metal ions. As a consequence, both of the specific capacity and operating voltage of the Li/NCM811 cells are decreased with repeatedly cycling. The results of this works also reveal that electrochemical oxidation of the electrolyte solvents and its resulting impact on the cell's impedance occur mainly in the initial charging, whereas the oxygen evolution and its relative adverse effects accompany whole life of the batteries. Most of the known problems with NCM811 material can be ultimately attributed to the oxidation of lattice oxygen (i.e., the oxygen evolution) and its relative reactions between the active oxygen evolution intermediates and electrolyte solvents. The conclusions of this work suggest that further research on NCM811 material should give priority to suppression of the oxygen evolution, followed by development of the anti-oxygen electrolytes that are chemically stable against the active oxygen evolution intermediates.

Acknowledgments

The author acknowledges the support of U.S. Army Research Laboratory, and thanks Dr. A. von Cresce for providing NCM811 cathode material and Dr. C. Lundgren for her

critical reading of the manuscript and valuable comments. Special appreciation is given to Dr. R. Jiang for his assistance in XRD measurement.

References

[1] A. Manthiram, J.C. Knight, S.T. Myung, S.M. Oh, Y.K. Sun, Adv. Energy Mater. 6 (2016) 1501010.
[2] F. Schipper, E.M. Erickson, C. Erk, J.Y. Shin, F.F. Chesneau, D. Aurbach, J. Electrochem. Soc. 164 (2017) A6220–A6228.
[3] S.T. Myung, F. Maglia, K.J. Park, C.S. Yoon, P. Lamp, S.J. Kim, Y.K. Sun, ACS Energy Lett. 2 (2017) 196–223.
[4] J. Kim, H. Lee, H. Cha, M. Yoon, M. Park, J. Cho, Adv. Energy Mater. 8 (2018) 1870023.
[5] H.J. Noh, S. Youn, C.S. Yoon, Y.K. Sun, J. Power Sources 233 (2013) 121–130.
[6] S.M. Bak, E. Hu, Y. Zhou, X. Yu, S.D. Senanayake, S.J. Cho, K.B. Kim, K.Y. Chung, X.Q. Yang, K.W. Nam, ACS Appl. Mater. Interfaces 6 (2014) 22594–22601.
[7] F. Lin, I.M. Markus, D. Nordlund, T.C. Weng, M.D. Asta, H.L. Xin, M.M. Doeff, Nat. Commun. 5 (2014) 3529.
[8] N.Y. Kim, T. Yim, J.H. Song, J.S. Yu, Z. Lee, J. Power Sources 307 (2016) 641–648.
[9] M. Dixit, B. Markovsky, F. Schipper, D. Aurbach, D.T. Major, J. Phys. Chem. C 121 (2017) 22628–22636.
[10] H.H. Ryu, K.J. Park, C.S. Yoon, Y.K. Sun, Chem. Mater. 30 (2018) 1155–1163.
[11] A. Tornheim, S. Sharifi-Asl, J.C. Garcia, J. Bareño, H. Iddir, R. Shahbazian-Yassar, Z. Zhang, Nano Energy 55 (2019) 216–225.
[12] R. Jung, M. Metzger, F. Maglia, C. Stinner, H.A. Gasteiger, J. Electrochem. Soc. 164 (2017) A1361–A1377.
[13] R. Jung, M. Metzger, H.A. Gasteiger, R. Jung, F. Maglia, C. Stinner, J. Phys. Chem. Lett. 8 (2017) 4820–4825.
[14] H. Liu, M. Wolf, K. Karki, Y.S. Yu, E.A. Stach, J. Cabana, K.W. Chapman, P.J. Chupas, Nano Lett. 17 (2017) 3452–3457.
[15] J. Wandt, A.T.S. Freiberg, A. Ogrodnik, H.A. Gasteiger, Mater. Today 21 (2018) 825–833.
[16] T. Teufl, B. Strehle, P. Muller, H.A. Gasteiger, M.A. Mendez, J. Electrochem. Soc. 165 (2018) A2718–A2731.
[17] K. Min, E. Cho, Phys. Chem. Chem. Phys. 20 (2018) 9045–9052.
[18] D.H. Cho, C.H. Jo, W. Cho, Y.J. Kim, H. Yashiro, Y.K. Sun, S.T. Myung, J. Electrochem. Soc. 161 (2014) A920–A926.
[19] P. Oh, B. Song, W. Li, A. Manthiram, J. Mater. Chem. A 4 (2016) 5839–5841.
[20] R. Jung, R. Morasch, P. Karayaylali, K. Phillips, F. Maglia, C. Stinner, Y. Shao-Horn, H.A. Gasteiger, J. Electrochem. Soc. 165 (2018) A132–A141.
[21] G. Assat, C. Delacourt, D.A.D. Corte, J.M. Tarascon, J. Electrochem. Soc. 163 (2016) A2965–A2976.
[22] K. Dai, J. Wu, Z. Zhuo, Q. Li, S. Sallis, J. Mao, G. Ai, C. Sun, Z. Li, W.E. Gent, W.C. Chueh, Y.D. Chuang, R. Zeng, Z.X. Shen, F. Pan, S. Yan, L.F.J. Piper, Z. Hussain, G. Liu, W. Yang, Joule 3 (2019) 518–541.
[23] W.S. Yoon, J. Hanson, J. McBreen, X.Q. Yang, Electrochem. Commun. 8 (2006) 859–862.
[24] Y.K. Sun, S.T. Myung, H.J. Bang, B.C. Park, S.J. Park, N.Y. Sung, J. Electrochem. Soc. 154 (2007) A937–A942.
[25] S.S. Zhang, Front. Energy Res. 2 (2014) 59, doi:10.3389/fenrg.2014.00059.
[26] L. Mu, R. Lin, R. Xu, L. Han, S. Xia, D. Sokaras, J.D. Steiner, T.C. Weng, D. Nordlund, M.M. Doeff, Y. Liu, K. Zhao, H.L. Xin, F. Lin, Nano Lett. 18 (2018) 3241–3249.
[27] J. Li, L.E. Downie, L. Ma, W. Qiu, J.R. Dahn, J. Electrochem. Soc. 162 (2015) A1401–A1408.
[28] J.R. Dahn, E.W. Fuller, M. Obrovac, U. von Sacken, Solid State Ion. 69 (1994) 265–270.
[29] Y. Wang, J. Jiang, J.R. Dahn, Electrochem. Commun. 9 (2007) 2534–2540.
[30] T. Hatsukade, A. Schiele, P. Hartmann, T. Brezesinski, J. Janek, ACS Appl. Mater. Interfaces 10 (2018) 38892–38899.
[31] R.D. Rauh, S.B. Brummer, Electrochim. Acta 22 (1977) 75–83.
[32] S.A. Freunberger, Y. Chen, Z. Peng, J.M. Griffin, L.J. Hardwick, F. Bardé, P. Novák, P.G. Bruce, J. Amer. Chem. Soc. 133 (2011) 8040–8047.
[33] J. Yang, Y. Xia, J. Electrochem. Soc. 163 (2016) A2665–A2672.
[34] S. Meini, N. Tsiouvaras, K.U. Schwenke, M. Piana, H. Beyer, L. Lange, H.A. Gasteiger, Phys. Chem. Chem. Phys. 15 (2013) 11478–11493.
[35] L. Zou, Z. Liu, W. Zhao, H. Jia, J. Zheng, Y. Yang, G. Wang, J.G. Zhang, C. Wang, Chem. Mater. 30 (2018) 7016–7026.
[36] S.S. Zhang, D.T. Tran, J. Power Sources 403 (2018) 167–172.
[37] L. Fan, D. Tang, D. Wang, Z. Wang, L. Chen, Nano Res. 9 (2016) 3903–3913.
[38] X.H. Yao, Q. Dong, Q.M. Cheng, D.W. Wang, Ang. Chem. Intern. Ed. 55 (2016) 11344–11353.
[39] N. Mahne, O. Fontaine, M.O. Thotiyl, M. Wilkening, S.A. Freunberger, Chem. Sci. 8 (2017) 6716–6729.
[40] W. Li, J.N. Reimers, J.R. Dahn, Solid State Ion. 67 (1993) 123–130.
[41] L. Wu, K.W. Nam, X. Wang, Y. Zhou, J.C. Zheng, X.Q. Yang, Y. Zhu, Chem. Mater. 23 (2011) 3953–3960.
[42] S. Hwang, D.H. Kim, K.Y. Chung, W. Chang, Appl. Phys. Lett. 105 (2014) 103901.
[43] S.K. Jung, H. Gwon, J. Hong, K.Y. Park, D.H. Seo, H. Kim, J. Hyun, W. Yang, K. Kang, Adv. Energy Mater. 4 (2014) 1300787.
[44] E. Flores, N. Vonrüti, P. Novák, U. Aschauer, E.J. Berg, Chem. Mater. 30 (2018) 4694–4703.
[45] M. Sathiya, K. Ramesha, G. Rousse, D. Foix, D. Gonbeau, A.S. Prakash, M.L. Doublet, K. Hemalatha, J.M. Tarascon, Chem. Mater. 25 (2013) 1121–1131.
[46] E. Hu, X. Yu, R. Lin, X. Bi, J. Lu, S. Bak, K.W. Nam, H.L. Xin, C. Jaye, D.A. Fischer, K. Amine, X.Q. Yang, Nat. Energy 3 (2018) 690–698.
[47] B.B. Berkes, A. Schiele, H. Sommer, T. Brezesinski, J. Janek, J. Solid State Electrochem. 20 (2016) 2961–2967.
[48] K. Min, S.W. Seo, Y.Y. Song, H.S. Lee, E. Cho, Phys. Chem. Chem. Phys. 19 (2017) 1762–1769.
[49] M. Dixit, B. Markovsky, D. Aurbach, D.T. Major, J. Electrochem. Soc. 164 (2017) A6359–A6365.
[50] Q. Xie, W. Li, A. Manthiram, Chem. Mater. 31 (2019) 938–946.
[51] T. Weigel, F. Schipper, E.M. Erickson, F.A. Susai, B. Markovsky, D. Aurbach, ACS Energy Lett. 4 (2019) 508–516.
[52] H.Y. Li, M. Cormier, N. Zhang, J. Inglis, J. Li, J.R. Dahn, J. Electrochem. Soc. 166 (2019) A429–A439.
[53] X. Fan, L. Chen, O. Borodin, X. Ji, J. Chen, S. Hou, T. Deng, J. Zheng, C. Yang, S.C. Liou, K. Amine, K. Xu, C. Wang, Nat. Nanotechnol. 13 (2018) 715–722.
[54] H.Q. Pham, E.H. Hwang, Y.G. Kwon, S.W. Song, Chem. Commun. 55 (2019) 1256–1258.
[55] Z. Zhu, A. Kushima, Z. Yin, L. Qi, K. Amine, J. Lu, J. Li, Nat. Energy 1 (2016) 16111.
[56] X. Liu, D. Ren, H. Hsu, X. Feng, G.L. Xu, M. Zhuang, H. Gao, L. Lu, X. Han, Z. Chu, J. Li, X. He, K. Amine, M. Ouyang, Joule 2 (2018) 2047–2064.
[57] S.S. Zhang, K. Xu, T.R. Jow, Electrochem. Solid State Lett. 5 (2002) A92–A94.
[58] S.S. Zhang, K. Xu, T.R. Jow, J. Electrochem. Soc. 149 (2002) A1521–A1526.
[59] F. Wu, J. Tian, Y. Su, J. Wang, C. Zhang, L. Bao, T. He, J. Li, S. Chen, ACS Appl. Mater. Interfaces 7 (2015) 7702–7708.
[60] T. Li, X. Li, Z. Wang, H. Guo, J. Power Sources 342 (2017) 495–503.
[61] X. Li, K. Zhang, M. Wang, Y. Liu, M. Qu, W. Zhao, J. Zheng, Sustain. Energy Fuels 2 (2018) 413–421.